Journal of Drug Delivery Science and Technology 110 (2025) 107123

Contents lists available at ScienceDirect

Journal of Drug Delivery Science and Technology

journal homepage: www.elsevier.com/locate/jddst

Solid-state characterization and solubility enhancement strategies for Olaparib in formulation development

Giuseppe Francesco Racaniello [a], Monica Pistone [a], Annalisa Cutrignelli [a], Corrado Cuocci [b], Rosanna Rizzi [b], Nunzio Denora [a], Antonio Lopalco [a,*], Angela Assunta Lopedota [a]

[a] Department of Pharmacy – Pharmaceutical Sciences, University of Bari, E. Orabona St. 4, 70125, Bari, (BA), Italy
[b] Institute of Crystallography-CNR, Amendola St. 122/o, 70126, Bari, (BA), Italy

ARTICLE INFO

Keywords:
Olaparib
Solid-state
Polymorphism
Solubility enhancement
Cyclodextrins
Soluplus®

ABSTRACT

During the formulation development of anticancer drug Olaparib (OLA), we observed that two batches (Batch 1 and Batch 2) obtained from the same supplier exhibited different solubility and dissolution behavior despite their identical chemical purity (99.9 %).

A comprehensive solid-state characterization was conducted. The Differential Scanning Calorimetry analysis showed distinct thermal behavior, with endothermic peaks at 202 and 215 °C, attributed to two polymorphic forms, as confirmed by Fourier Transform Infrared Spectroscopy and Thermogravimetric Analysis. Powder X-ray Diffraction analysis revealed that Batch 1 contained a mixture of OLA Form A (major) and Form L (minor, ~15 % w/w), and exhibited lower crystallinity compared to Batch 2. Batch 2 consisted exclusively of pure OLA Form L, whose crystal structure was reported here for the first time. Morphology analysis indicated that Batch 1 presented particles with heterogeneous dimensions (2–60 μm), while Batch 2 showed a homogeneous size distribution (~5 μm), resulting in differences in density and specific surface area. These differences in solid-state properties further contributed to observed variations in equilibrium solubility and intrinsic dissolution rate (IDR), with Batch 1 exhibiting a higher solubility and IDR (0.1239 mg/mL; 26.74 mg/cm^2·min^{-1}) than Batch 2 (0.0609 mg/mL; 13.13 mg/cm^2·min^{-1}) at 37 °C.

The addition of Soluplus® and hydroxypropyl-β-cyclodextrin significantly enhanced OLA solubility in concentration-dependent manner, up to 1.2-fold and 12-fold for Batch 1 and 2.5-fold and 26-fold for Batch 2, respectively, after 72 h of incubation. These findings demonstrate that, despite initial differences in polymorphic composition and particle morphology, appropriate solubilizing agents can mitigate batch-to-batch variability and optimize OLA solubility.

1. Introduction

In recent years, to reduce costs, many pharmaceutical companies have outsourced manufacturing to external suppliers, leading to stricter regulations and increased scrutiny of Active Pharmaceutical Ingredients (APIs) production and characterization [1,2]. Beyond chemical composition, the solid-state properties of an API play a crucial role in formulation, influencing solubility, dissolution rate, stability, processability, and overall drug performance. Proper solid-state characterization is therefore essential to prevent formulation issues, optimize drug development, and reduce production costs and time [3]. However, technical data sheets provided by suppliers often focus primarily on the chemical characteristics of the substance, offering limited information about its solid-state properties. Since these properties are fundamental to bioavailability, it is essential to investigate them thoroughly before pharmaceutical application. Over the past five decades, preformulation studies have become a cornerstone in pharmaceutical development, introducing a more scientific and systematic approach to formulation design [1]. These studies focus on evaluating the physicochemical and biopharmaceutical properties of APIs and their interactions with excipients. A key aspect of preformulation is the solid-state characterization of the drug, including assessments of crystallinity, polymorphism, hygroscopicity, and particle size, as well as the evaluation of solubility and intrinsic dissolution rate (IDR) [3,4]. Understanding these properties is critical in improving drug solubility, permeability, and stability, ultimately aiding in the selection of suitable excipients and

* Corresponding author.
E-mail address: antonio.lopalco@uniba.it (A. Lopalco).

https://doi.org/10.1016/j.jddst.2025.107123
Received 26 November 2024; Received in revised form 26 May 2025; Accepted 29 May 2025
Available online 29 May 2025

manufacturing conditions for optimized pharmaceutical formulations [4]. Olaparib (OLA) (see Fig. 1), a PARP (poly ADP ribose polymerase) inhibitor, exemplifies the challenges associated with low aqueous solubility and limited permeability, classifying it as a BCS Class IV drug [4,5]. Despite these drawbacks, OLA has demonstrated significant therapeutic efficacy against various tumors and has been approved by regulatory agencies for treating ovarian, prostate, and breast cancers [6]. The commercial formulations of OLA include Lynparza® capsules and tablets, featuring the drug in either a micronized crystalline form (dispersed in lauroyl macrogol-32 glycerides) or an amorphous form (embedded in a copovidone-based polymer matrix) to enhance solubility and bioavailability [7]. However, the capsule formulation requires a high daily dosage (16 units of 50 mg each), increasing the risk of adverse effects [8], while the amorphous tablet formulation, though more bioavailable, poses stability and large-scale manufacturing challenges [7,9,10]. API batches identified as 99.9 % chemically pure by suppliers can exhibit significant variability in their physical properties, leading to inconsistencies in formulation performance despite following identical protocols. Studying the solid-state properties of an API and its behavior in aqueous environments, especially in terms of solubility and IDR, is fundamental for designing an effective dosage form [3]. OLA is known to exist in two anhydrous polymorphic forms (Form A and Form L), which have been described in two patents [11,12]. Form A, typically obtained via crystallization from ethanol/water or methanol/water mixtures, is the one selected for commercialization. This polymorph exhibits a higher melting point (~210 °C) and is readily formed under manufacturing conditions. Form L, which can also crystallize from similar solvent systems, shows a lower melting point (~198.5 °C) and has been observed to recrystallize to Form An upon heating, suggesting a thermally induced transition [13,14]. These forms differ significantly in their physiochemical properties, with Form A being more soluble than Form L. Due to its higher solubility, Form A is the preferred polymorphic form in the marketed Lynparza capsules. However, routine quality control of commercial batches has revealed that levels of Form L above 20 % within Form A may affect drug efficacy, as such concentrations are sufficient to reduce the solubility of the active substance [15].

Given the importance of polymorphic identity on solubility, stability, and bioavailability, a thorough understanding of the crystalline forms and solid-state properties of each batch is essential. Despite the pharmaceutical relevance of these crystalline polymorphs, previous research has focused primarily on thermal analysis and on a qualitative interpretation of powder X-ray diffraction (PXRD) patterns, without providing a full structural elucidation of these crystalline forms. In contrast, in this study, we provide, for the first time, a full powder structure determination of Form L. To our knowledge, this is the first work to offer such a characterization, providing structural insights that support a broader understanding of its physicochemical properties.

In this study, we investigated the solid-state characteristics of two batches of OLA (Batch 1 and Batch 2), identifying distinct differences in their crystalline, thermal, and micromeritic properties by using analytical techniques, including PXRD, Fourier Transform Infrared Spectroscopy (FT-IR), Differential Scanning Calorimetry (DSC), Thermogravimetric Analysis (TGA), and morphological assessments. These analyses provided valuable insights into the crystal structure, thermal stability, and molecular interactions that influence the drug's physicochemical properties. Notably, we report for the first time, the identification of a polymorphic mixture (Form A and L) in one of the commercial batches of Olaparib, with associated implications for solubility and dissolution behavior.

Furthermore, solubility and dissolution studies in aqueous environments of the two batches were conducted to assess the impact of solid-state differences. Given low solubility of OLA, phase solubility studies were performed in the presence of two solubilizing agents - Soluplus® (SOL) and hydroxypropyl-β-cyclodextrin (HP-β-CD) (see Fig. 1) to evaluate their potential in enhancing drug solubility and bioavailability. This research aims to highlight the importance of preliminarily evaluating the solid-state properties of the purchased APIs, in the specific case of the two batches of OLA powders and provide a scientific foundation for optimizing its pharmaceutical formulation, ultimately improving its therapeutic effectiveness.

2. Materials and methods

2.1. Materials

Two batches of OLA were purchased from Cabru s.a.s. (Arcore, Italy). HP-β-CD (DS = 7.5, MW = 1480 Da, molar substitution 0.88) was donated by Farmalabor Srl (Canosa di Puglia, Italy). SOL (polyvinyl caprolactam-polyvinyl acetate-polyethylene glycol graft co-polymer) was donated by BASF (Ludwigshafen am Rhein, Germany). For the analysis, distilled water (conductivity of 18.2 MΩ cm at 23 °C) was obtained by the purification system Milli-Q (Purelab DI, MK2) (Elga, High Wycombe, UK). Methanol for HPLC was purchased by Sigma Aldrich Italy (Milan, Italy).

2.2. Solid-state characterization studies

2.2.1. FT-IR spectroscopy, TGA and DSC analyses

The solid-state study of the two different batches (Batch 1 and Batch 2) of the drug was carried out using FT-IR, TGA, and DSC. The density and specific surface area of the two batches were also investigated.

KBr pellets with ~2 % of each sample were examined by the FT-IR 1600 PerkinElmer spectrophotometer for FT-IR analysis. The data was collected between 4000 cm^{-1} and 400 cm^{-1}.

The PerkinElmer Thermogravimetric Analyzer Pyris 1 TGA was employed to conduct TGA analysis on the pure drug. Each sample (~9 mg) was placed into platinum pans and heated at a rate of 10 °C/min to achieve a temperature of 600 °C. The thermal decomposition (or degradation) profile was examined using PyrisTM software version 11. During the trials, the nitrogen (N_2) gas flow rate was 20 mL/min. Thermal DSC analysis of the powders was carried out using PerkinElmer DSC 4000 equipment. The enthalpy and temperature were calibrated

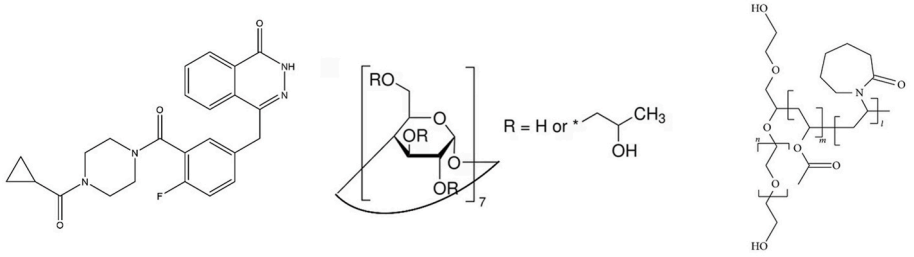

OLAPARIB **HP-β-CD** **SOLUPLUS®**

Fig. 1. Chemical structure of the active ingredient OLA and the solubilizing agents HP-β-CD and SOL.

using Indium as a standard and blank control. The samples (5–10 mg) were placed in an aluminum pan with a 40 mL capacity and 0.1 mm thickness, after which they were covered with perforated aluminum lids. Finally, they were heated from 0 to 230 °C at a 10 °C/min rate. Furthermore, additional scans were performed for each sample using multiple heating and cooling cycles, which included an initial heating phase from 30 °C to 230 °C at a rate of 10 °C/min, followed by a subsequent cooling phase from 230 °C to 30 °C at a rate of 20 °C/min and finally, a further heating phase in the same temperature range and at the same rate as the first phase.

Subsequently, the two samples were again investigated using multiple heating and cooling cycles scans to highlight the differences between the peaks noted. The new scans were carried out through a first heating phase from 30 °C to 210 °C at a rate of 2 °C/min (90 min), followed by an isothermal scan at 210 °C for 10 min, a subsequent cooling phase from 210 °C to 30 °C at a rate of 2 °C/min (90 min) and finally a new heating phase from 30 °C to 240 °C at a rate of 2 °C/min (110 min). During each analysis N_2 was used as purge gas at a 20 mL/min rate.

2.2.2. Powder density and specific surface area

The density of the two batches was measured using the Anton Paar Ultrapyc 5000 gas pycnometer (Anton Paar, Graz, Austria). To perform the measurement, the powder was poured into a microcell of known volume (10 cm^3) and the system was subsequently weighed and inserted into the instrument. The experiment was conducted at a controlled temperature of 25 °C and under N_2 flow with a controlled pressure in the measuring chamber of 4.205 psi.

The identified densities were used to assess the specific surface area of the powders using a Manual Blaine Air-Permeability Apparatus (Testing Bluhm & Feuerherdt GmbH, Berlin, Germany) [16]. Briefly, a filter paper disc was placed over the perforated metal disc of the permeability cell. The powder was weighed and transferred to the permeability cell for examination. The cell was leveled to even out the surface of the powder bed and covered with a second filter paper disc employing a 10 g plastic pencil without applying pressure. The permeability cell was attached to the manometer tube and the tightness of the system created was verified. The air from the pressure gauge was evacuated using a rubber bulb until the liquid level was at its highest point. With the help of a timer, the time required for the liquid to drop from the second to the third mark on the pressure gauge was measured. The operation was repeated three times to measure the time taken for the air to flow through each powder bed and all samples were under the same temperature and humidity conditions.

The specific surface area per unit of mass (S_w) of the investigated Batch 1 and Batch 2 powders expressed in [cm^2/g] was obtained through the following Equation (1):

$$S_w = \frac{K}{\rho} \times \frac{\sqrt[2]{e^3}}{1-e} \times \frac{\sqrt[2]{t}}{\sqrt[2]{10 \times \eta}} \quad (1)$$

where K is the apparatus constant determined experimentally by identifying the volume of the powder load cell (equal to 19.49 $g/cm^2 \times s^2$), e is the porosity (equal to 0.5), ρ represents the density of the powder, η is the air viscosity at 20 °C (equal to 0.00001819 Pa × s) and t represents the recorded flow time in seconds.

2.2.3. Scanning electron microscopy and PXRD

Morphological analyses of the powders were conducted by Scanning electron microscopy (SEM) by using a SEM HITACHI TM3000 with DEBEN "Tilt & Rotate Sub-Stage," setting the accelerating voltage at 15 Kv, the vacuum values at $5x10^{-3}$ Pa and the working distance at 6.60 mm.

The crystal structure characterization was performed using PXRD data. The diffraction patterns of Batch 1 and 2 were collected at room temperature using a Rigaku Rint2500 laboratory diffractometer equipped with a rotating Cu anode. The instrument, operated at 50 kV and 200 mA in Debye-Scherrer geometry, used an asymmetric Johansson Ge (111) crystal to select monochromatic CuKα_1 radiation (λ = 1.54056 Å), along with the silicon strip Rigaku D/teX Ultra detector. The data were collected in the 7 to 65° (2ϑ) range, with a step size of 0.02° (2ϑ) and a counting time of 6 s/step. For the measurements, the powder sample was placed in a 0.5 mm diameter glass capillary, which was mounted on the goniometer's axis. The capillary was rotated during the measurement to enhance the randomization of the individual crystallites' orientations and minimize the potential effect of preferred orientation.

The crystal structure was determined using the EXPO software [17] in a fully automated process, following the standard steps of polycrystalline structure determination. This includes calculating the unit cell parameters, identifying the space group, solving the structure, and refining the model using the Rietveld method [18]. Specifically, the N-TREOR09 software [19], as integrated into EXPO, was used to index the powder pattern by selecting and fitting the first 25 well-defined low-angle peaks. The unit cell parameters that gave the highest figure of merit (M_{20} = 36), successfully indexed all peaks with a monoclinic cell. Systematic absences suggested the space group $P2_1/c$ as the most probable one. The crystal structure determination was performed in direct space [20] using the Simulated Annealing (SA) algorithm implemented in EXPO. The initial starting model was constructed with the sketching facilities of ACD/ChemSketch (ACD/ChemSketch, 2003), and geometrically optimized with the MOPAC2016 program (MOPAC2016, 2016). The SA relies on minimizing the difference between observed and calculated intensities by adjusting the position, orientation, and conformation of an expected molecular model within the unit cell. The angular range of $7° < 2\theta < 45.3°$ (2.0 Å resolution) was used. During the minimization process, EXPO optimized a total of 12 parameters (DOFs), including 3 coordinates for the position of centers of mass, 3 angles for orientation, and 6 torsion angles for conformation. The algorithm was run 100 times under a Linux workstation in default mode and parallel calculation over 40 CPUs. The most favorable solution, yielding the lowest cost function (R_{wp} = 6.26), was selected. The acceptance criterion also considered the integrity of crystal packing. The hydrogen atom positions were improved by using the density-functional theory (DFT) geometry optimization performed with Quantum ESPRESSO software [21]. The resulting crystal structure solution served as the initial model for the Rietveld refinement. Non-hydrogen atoms were refined anisotropically. All the hydrogen atoms bonded to carbon atoms were placed at calculated positions and refined isotropically using a riding model approximation under the constraint on atomic displacement parameters Uiso(H) = 1.2Uiso(C). Pearson VII function was employed to model the peak shape, and the atomic displacement parameters were isotropically refined, and constrained to have consistent values for atoms of the same chemical element.

To validate the refined crystal structure, periodic, solid-state calculations performed by Quantum ESPRESSO, an *ab initio* quantum-mechanical program employing plane waves and density-functional theory to simulate the properties of solids, were executed. The following execution parameters were used: PBE potentials from the SSSP Efficiency PBE (version 1.1) library [22], a cut-off parameter set to 60 Ry to control calculation accuracy, k-point spacing was 0.15 $Å^{-1}$, van der Waals interactions were corrected employing a Grimme's D3 dispersion correction [23]. Only the atomic coordinates of the structure were optimized using the experimental cell parameters and atomic positions obtained from the Rietveld refinement. The root-mean-square (RMS) displacements of non-H atoms between the DFT-optimized and experimental crystal structure was 0.050 Å, providing strong evidence for the correctness of the experimental structure [24]. X-ray Crystallographic Information file OLA-L_file001.cif contains the supplementary crystallographic data for this paper, and is supplied as an independent Supporting Information file for this article. This file can also be obtained free of charge from the Cambridge Crystallographic Data Centre via www.cc

dc.cam.ac.uk/data_request/cif <http://www.ccdc.cam.ac.uk/data_request/cif> (CCDC 2337326).

The previously described structural characterization refers to Batch 2, which was confirmed to be a pure phase, whereas the crystal structure characterization of Batch 1 was not feasible due to its composition as a mixture of two crystalline phases.

2.3. OLA behavior in aqueous environment

2.3.1. High-pressure liquid chromatography method for OLA concentration determination

High-pressure liquid chromatography (HPLC) determination of OLA was performed using Shimadzu HPLC Nexera series, equipped with SPD-M40 photodiode array detector, SIL-40C autosampler, and CTO-40C column oven. For evaluation, a Zorbax C18 column (150 mm × 4 mm; 5 μm particles) was eluted in isocratic mode with a mixture of methanol and deionized water (64:36 v/v), constantly monitoring the eluent at 276 nm. A flow rate of 1 mL/min and a column temperature of 30 °C were utilized, resulting in the elution of the drug at a time of 3.21 min (min). The assay was performed by injecting a 20 μL volume of each sample. The data analysis was processed using LabSolutions version 5.111 Shimadzu Corporation.

For the determination of the concentration of OLA in water, a calibration curve was performed in the 0.5 μg/mL - 100 μg/mL range, and a linear plot ($R^2 = 0.999$) was produced.

2.3.2. Equilibrium aqueous solubility determination of OLA

The study evaluating the equilibrium aqueous solubility of the drug from Batch 1 and Batch 2 was conducted by placing an excess of the API inside vials containing 2 mL of distilled water (pH 6.0). Samples were placed inside a thermostatically controlled bath at 37 ± 0.5 °C and a climatic chamber at 25 ± 0.5 °C. Samples were analyzed at 24, 48, 72, 96 and 168 h (h), after being centrifuged at 13000 rpm for 10 min at 37 °C or 25 °C respectively and the supernatant was diluted 1:100 in a mixture of methanol/water (64:36 v/v). HPLC analysis of all samples was conducted in triplicate.

2.3.3. Dissolution profile of the powders in water

The dissolution studies of the powders from the two batches were conducted in distilled water (pH 6.0) for 8h and in an acidic environment simulating gastric pH conditions (0.1 M HCl, pH 1.2) for 2h, to investigate potential differences shown by the samples. Both analyses were conducted in triplicate using a Vankel paddle dissolution tester USP II model VK 7000 (Varian, Inc., U.S.), setting the paddle speed at 100 rpm and the vessel temperature at 37 ± 2 °C. Briefly, 5 mg of OLA from Batch 1 and Batch 2 were weighed, and subsequently placed in a vessel with a volumetric capacity of 900 mL of distilled water or 0.1 M HCl medium. 5 mL samples were then taken at determined intervals of time until the end of the analysis and each sample was replaced with an equal volume of appropriate medium. Finally, samples from both dissolution studies were analyzed by HPLC for drug concentration determination.

2.3.4. Intrinsic dissolution rate profile of the powders in water

The IDR method assessed the different drug dissolution profile from Batch 1 and Batch 2. For the test, a slightly modified version of a method previously used in the literature was employed [25]. Briefly, 100 mg of pure powder sample were pressed within the test apparatus using a 15 Ton Hydraulic KBr Press (PerkinElmer, Waltham, Massachusetts, US) resulting in a cylindrical tablet of 14 mm diameter. The resulting tablets were inserted into a cylindrical steel tube of the same diameter (14 mm) with open ends. Thus, the system was suspended inside a vane dissolver so that only one side of the tablet remained exposed to the solvent. The dissolution medium was 900 mL of water solution, and the temperature was maintained at 37 ± 0.5 °C [25]. At scheduled intervals, samples were taken from the dissolution vessel, which were subsequently analyzed by HPLC to assess the amount of OLA in solution using the above-described method. When the amount of dissolved drug (mg/mL) is expressed as a function of time (min), the slope of this curve gives the IDR. Three parallel experiments were recorded. The IDR of the OLA was determined through Equation (2) below:

$$IDR = V \times \frac{k}{A_{disc}} \quad (2)$$

Where V is the volume of the medium (mL), k is the initial slope of the dC/dt curve (concentration in mg/mL per time unit), and A_{disc} is the total surface area of the produced disc (cm^2).

2.4. Phase solubility in the presence of HP-β-CD and SOL

The phase solubility study of OLA from Batch 1 and Batch 2 in the presence of two different solubilizing agents HP-β-CD and SOL was performed according to the Higuchi-Connors method [26,27]. Briefly, 2 mL samples containing solutions at various concentrations of HP-β-CD were prepared, covering a concentration range from 14 to 112 mM. An excess amount of drug was placed inside each solution, and the resulting suspensions were mixed for 2 min. Similarly, an excess of the drug was placed inside vials containing aqueous solutions of equal volume (2 mL) and at different SOL concentrations. These concentrations were in the range of 3.39–67.8 mM. Subsequently, all the samples were allowed to rest in a thermostatic bath at 37 ± 0.5 °C at a constant oscillation for 24, 48, and 72h. Hence, the samples were centrifuged at 13000 rpm for 10 min at 37 °C and the supernatant was analyzed. The solubility diagram was obtained by plotting the molar concentration of the drug against the HP-β-CD or SOL molar concentration.

2.5. Statistical analysis

The results are expressed as the mean ± SD from three independent experiments. For equilibrium aqueous solubility data, statistical significance was calculated using a two-way analysis of variance (ANOVA) followed by the Bonferroni post hoc tests (GraphPad Prism version 5.0 for Windows, GraphPad Software, San Diego, CA). Differences were considered statistically significant at $p < 0.05$*.

3. Results and discussion

3.1. Solid-state characterization studies

The solid-state characterization studies of two purchased OLA batches, performed by a detailed investigation of granulometry and particles morphology, powder density, and specific surface area, revealed differences in their physical properties. Further analysis, performed via FT-IR, TGA and DSC, supported the hypothesis of the presence of two polymorphic forms of the API. PXRD analysis confirmed these polymorphs, previously identified in the literature as Form A and Form L [11,12].

3.1.1. FT-IR spectroscopy, TGA and DSC analyses

In the present study, FT-IR spectroscopy was employed to assess possible variations in the solid physical state of OLA in the two batches. These variations may depend on the different degrees of crystallinity and the alteration of hydrogen bonds, which describe specific vibrational frequencies resulting in frequency shifts and/or subdivision of absorption peaks [28]. Although for both OLA batches, it is possible to note the symmetrical elongation vibration at 3170 cm^{-1} related to the N-H bond of the amide group and the elongation vibration at 1660 and 1630 cm^{-1} corresponding to the C=O group [29], there are some differences between the two spectra (Fig. 2). The first powder spectrum (Batch 1) shows the stretching bands of the N-H group more diffuse and broadened, as well as a slight shift towards lower frequencies of the C=O

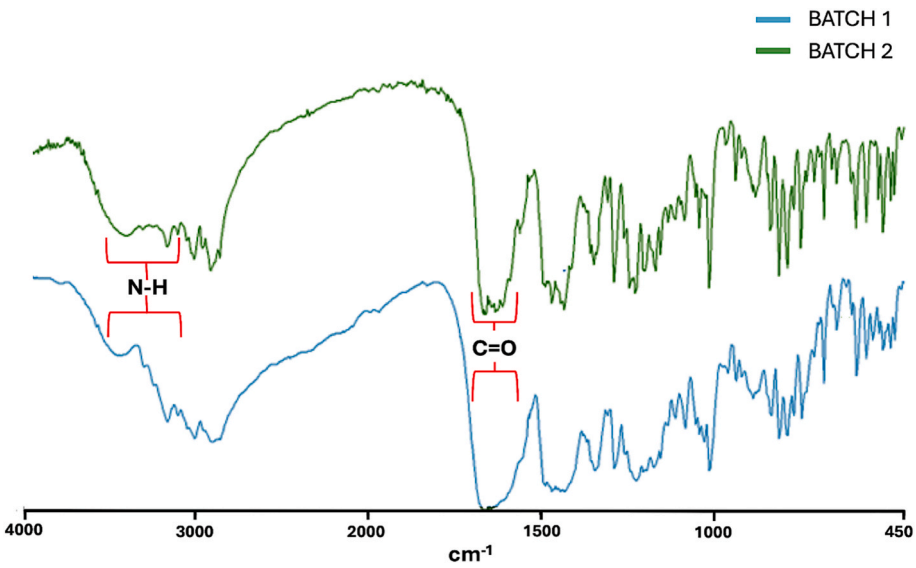

Fig. 2. FT-IR spectra of Batch 1 (green) and Batch 2 (blue). (For interpretation of the references to colour in this figure legend, the reader is referred to the Web version of this article.)

group. This behavior may be related to the lower degree of crystallinity of Batch 1 compared to Batch 2, as later indicated by the X-ray diffraction patterns, which will be described and discussed in detail in the following sections.

Moreover, the thermal behavior of the samples was studied utilizing TGA and DSC analysis. As can be seen from Fig. 3, the TGA curves for the powders overlap and shows an absence of weight loss before decomposition, indicating that no water or residual solvent is present [30]. This finding excludes the presence of pseudopolymorphic forms (e.g., hydrates or solvates) and confirms that both samples were constituted by anhydrous polymorphs. The degradation temperature of both batches is around 300 °C, as confirmed by other works in the literature [29]. However, it is possible to identify a small difference in the temperature of onset of degradation, which turns out to be lower in the Batch 2 sample (~270 °C) than in Batch 1 (~310 °C). This result suggests the presence of two different solid states of the drug in the batches investigated, with a higher stability of one than the other.

DSC analyses were performed to investigate the thermal behavior of the two OLA batches and to assess the presence of different polymorphic forms as well as their ability to generate a stable amorphous phase. DSC analysis was performed in multiple stages: initially to observe the melting behavior, followed by cycling to assess recrystallization, and finally to investigate the potential transformation of Form L into Form A. This sequence of analyses allowed for a detailed characterization of the thermal behavior and the polymorphic transitions between the two forms. Multiple heating and cooling cycles were employed to assess the thermal behavior and stability of the polymorphs.

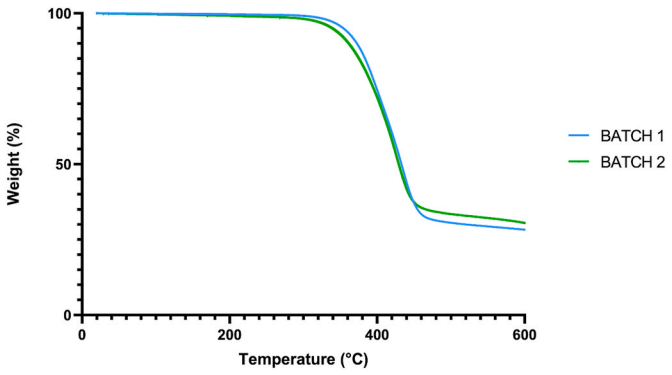

Fig. 3. The TGA curves for Batch 1 and Batch 2.

The DSC thermogram of Batch 1 displayed a small endothermic peak around 202 °C followed by a second one at around 215 °C, while Batch 2 showed two distinct and more intense endothermic peaks at the same temperatures (Fig. 4A). According to the literature data, the endothermic peak at 215 °C corresponds to the melting of Form A of OLA [12], whereas the peak at 202 °C is associated with Form L [11]. This assignment is in agreement with previous reports, that described the thermal behavior of multiple OLA polymorphs.

To further investigate the thermal behavior of the two forms, DSC analyses were conducted using multiple heating and cooling cycles at 5 °C/min for the heating steps and 10 °C/min for the cooling step. After reaching the melting point, neither form exhibited recrystallization during the cooling phase, nor during the subsequent heating cycle, as shown in Fig. 4B. Notably, a clear glass transition was observed, without the appearance of exothermic recrystallization peaks typically associated with the crystalline drug forms.

The absence of recrystallization during both cooling and subsequent heating cycles substantiates the classification of both forms as Glass Forming Ability (GFA) Class III materials, as described by Baird et al. [31], which refers to amorphous materials that do not show recrystallization upon thermal cycling and exhibit amorphous stability. The generation of a stable amorphous phase under thermal stress is a favorable feature for formulation development [31,32].

Finally, an additional DSC experiment was conducted using a reduced heating and cooling rate of 2 °C/min to enhance resolution of thermal transitions (Fig. 5A–D). The new scans were carried out through a first heating phase from 30 to 210 °C at a rate of 2 °C/min (90 min), followed by an isothermal scan at 210 °C for 10 min, a subsequent cooling phase from 210 °C to 30 °C at a rate of 2 °C/min (90 min) and finally a new heating phase from 30 °C to 240 °C at a rate of 2 °C/min (110 min). The aim of this experiment was to assess whether exposure to high temperatures could induce the transformation of Form L into the crystalline Form A.

As shown in Fig. 5A, upon heating both samples from 30 °C to 210 °C, an endothermic peak at 200 °C and an exothermic peak at 202 °C were observed only in Batch 2, corresponding to the melting of Form L and to a possible recrystallization of the polymorph in Form A, respectively. An onset point of the melting peak of Form A at around 206 °C was also observed in the thermogram. In contrast, the thermogram of Batch 1 showed only the onset point of the melting peak of Form A at around 206 °C. Both samples were then held at 210 °C for 10 min and

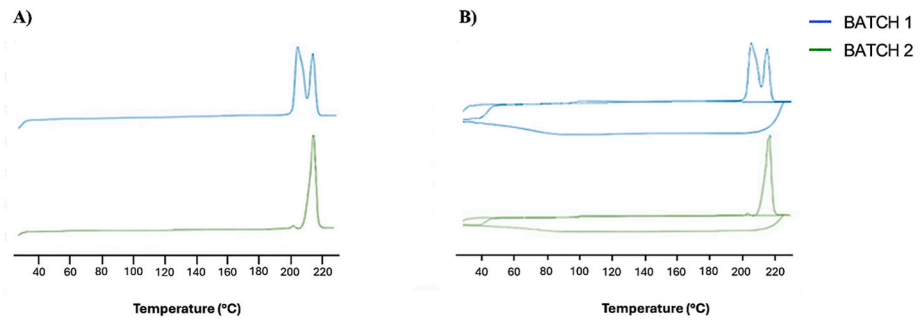

Fig. 4. DSC thermograms of powders from Batch 1 and 2 (a) and their DSC scans using multiple heating and cooling cycles (b).

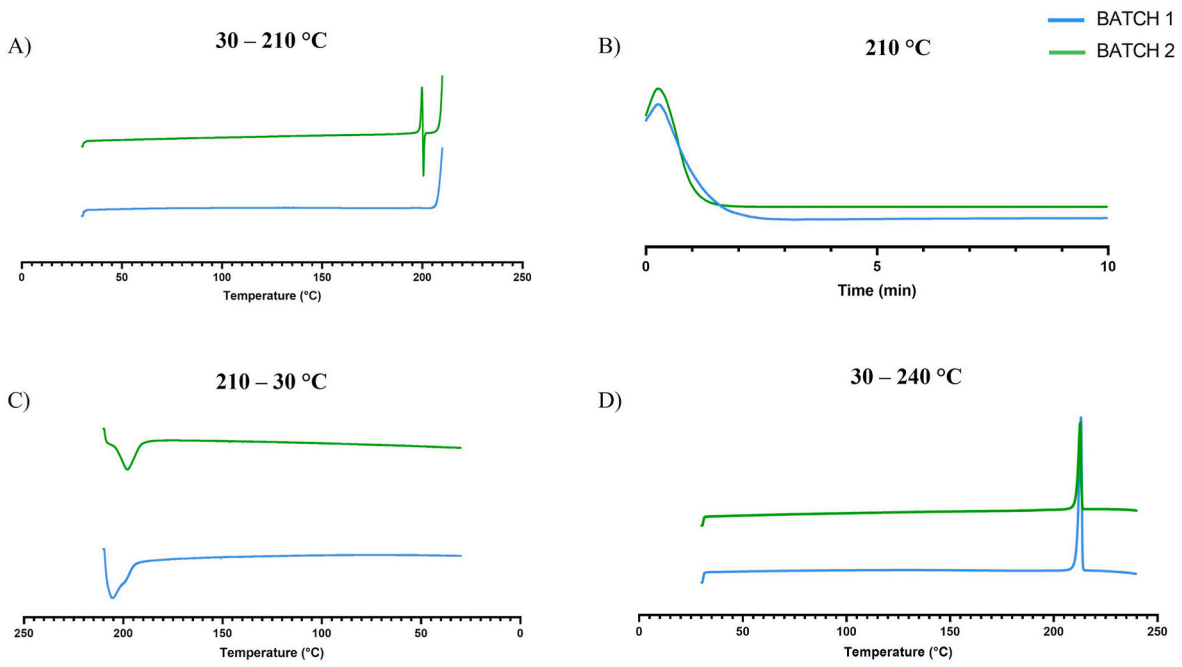

Fig. 5. DSC scans of OLA in Batch 1 and 2 using multiple heating and cooling cycles of 30 °C–210 °C thermogram (A), isothermal at 210 °C for 10 min (B), of 210 °C–30 °C (C), and 30 °C–240 °C (D) thermograms.

subsequently cooled to 30 °C at a rate of 2 °C/min (Fig. 5B and C). During this isothermal hold, one can still discern, in the first minutes of exposure to the set temperature, the onset of melting of Form A, with no further baseline shifts for the remaining time (Fig. 5B).

During cooling of the sample to 30 °C at a rate of 2 °C/min, two minor exothermic events can be observed (at ~200 °C for Batch 2 and

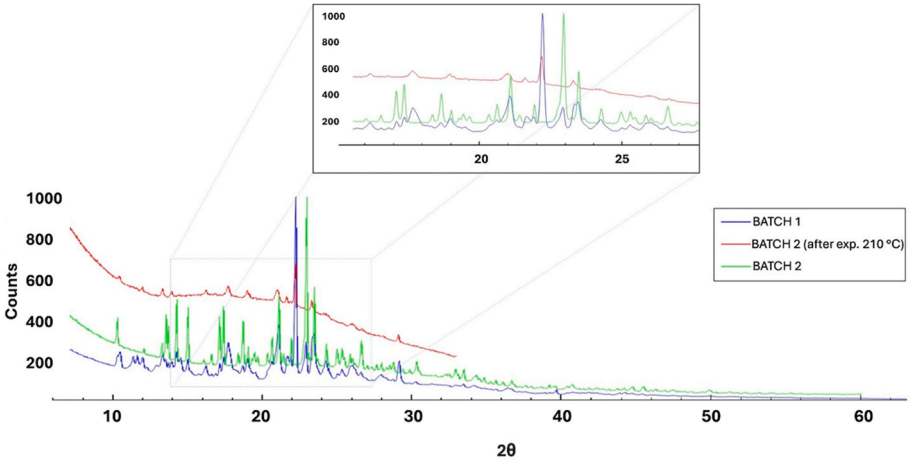

Fig. 6. Powder X-ray diffraction patterns of Batch 1 (blue), Batch 2 (green), and Batch 2 after prolonged exposition at 210 °C (red). (For interpretation of the references to colour in this figure legend, the reader is referred to the Web version of this article.)

~205 °C for Batch 1) (Fig. 5C), attributable to a structural rearrangement and the partial presence of amorphous material in the batches following the partial melting phase, which began at 206 °C and was held isothermally at 210 °C. This is further confirmed by the diffractogram shown in Fig. 6 for Batch 2 after exposure to 210 °C for 10 min. The presence of an elevated baseline and the less defined diffraction peaks indicate that the content of the powder in Batch 2 held to 210 °C for 10 min was partially crystalline and amorphous.

In the second heating cycle up to 240 °C (Fig. 5D), both batches exhibited a single endothermic peak at approximately 215 °C, which is characteristic of Form A. These observations suggest that Form L converts into Form An upon thermal exposure. This behavior is indicative of a monotropic polymorphic system, in which one form is thermally more stable at all temperatures. In such systems, the less thermal stable Form L tends to irreversibly transform into the thermal stable Form An upon heating, typically without exothermic events related to crystallization [33].

3.1.2. Crystallographic study: PXRD characterization of batch 1 and batch 2

The X-ray powder diffraction data collected from both samples were analyzed to carry out their structural characterization. In Fig. 6, the diffraction patterns of Batch 1 and 2 are shown in blue and green, respectively. According to patents on OLA polymorphs [11,12], Form A [12] is characterized by distinct peaks at 2θ values of 12.0, 17.8, 21.1, 22.3, and 29.2, while Form L [11] exhibits characteristic peaks at 14.4, 17.2, 17.5, 18.8, and 23.0. The absence of an elevated baseline and the presence of well-defined diffraction peaks indicate that both Batch 1 and Batch 2 are crystalline, with no evidence of significant amorphous content detectable by PXRD. Fig. 7 compares the experimental powder diffraction pattern of Batch 1 with the reference peak positions listed above for both Form A (vertical purple markers) and Form L (vertical green markers), while Fig. 8 shows the diffraction pattern of Batch 2 with only the characteristic peaks corresponding to Form L (vertical purple markers).

This comparison clearly indicates that Batch 2 corresponds to pure Form L, whereas Batch 1 exhibits peaks associated with both Form A and Form L, indicating the presence of a polymorphic mixture.

The phase fraction of the L-phase within the mixture was estimated based on the assumption that no matrix effects apply to the polymorphic mixture of the same compound. In this case the diffracted intensity of a given phase is directly proportional to its concentration [34]. From the scaling factor applied to the pure L-phase powder pattern to match the L-phase peaks in the L- and A-mixture pattern recorded under the same conditions, the L-phase fraction was determined to be approximately 15 % w/w. This procedure is also known as the external standard method [34].

These findings further validate the existence of two distinct OLA polymorphs and support the conclusions drawn from previous solid-state analyses.

To test the hypothesis from the DSC study, that prolonged high-temperature exposure could convert Form L into the more stable Form A, a PXRD data collection was also performed on the Batch 2 sample heated at 210 °C for 10 min. In Fig. 6, the diffraction pattern of this heated sample (in red) shows characteristic peaks of Form A, including the most intense at 2θ = 22.3°, while the peaks specific to Form L disappear.

The heated compound exhibits a predominantly amorphous structure, with only residual crystallinity corresponding to peaks matching those of Form A. The broad background and reduced peak intensity suggest that the 10-min heat treatment at 210 °C is sufficient to induce amorphization, although not completely. For clarity, a magnified view of the relevant diffraction range is included. This confirms that extended heating leads to transformation into Form A and significant amorphization. In terms of crystal structure characterization, this study represents the first structural determination of Form L, as there are no previous reports in the literature providing a full structural analysis of this polymorph, though the existence of Form L has been noted in patents and other studies [12,14]. A full structure solution was successfully achieved for Batch 2, with the unit cell and crystallographic parameters reported in Table 1. The main X-ray data and acquisition parameters are reported in Table S1.

The refined crystal structure is illustrated in Fig. 9a and b. The crystal packing is mainly stabilized by van der Waals forces. A contribution to the stability of the crystal packing arises from π-π stacking interactions between the aromatic rings of symmetry-related molecules, with a centroid-to-centroid distance of 5.58 Å for the strongest interaction between the phenyl rings that are part of the phthalazinyl groups.

3.1.3. Powder density and specific surface area

Density and specific surface area studies of the powder highlighted a difference between the two batches. The data collected in Table 2 shows that the powder in Batch 2 was characterized by a higher density and specific surface area compared to the other. The higher density suggests that the particles of this batch are more tightly packed or possess a different crystalline structure compared to the other. This could impact the bulk and tap densities of the powders, influencing properties such as flowability and compaction behavior during the formulation processes of solid dosage forms (blending, tableting, or encapsulation) and homogeneity of the API in the final formulation. Powder in Batch 2 also shows a higher specific surface area. A greater specific surface area generally means more surface available for interaction with solvents,

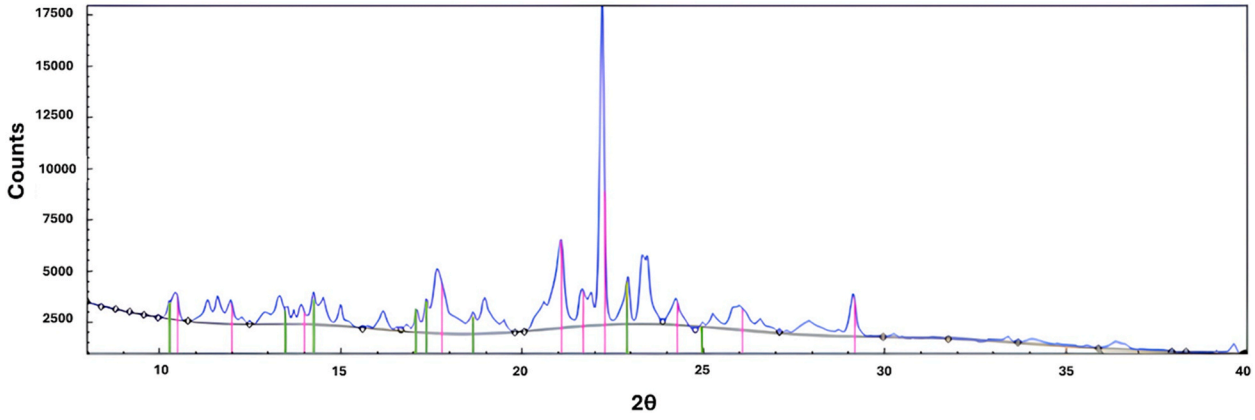

Fig. 7. Powder X-ray diffraction pattern of Batch 1, with the positions of specific and characteristic peaks, as reported in the patents [11,12], highlighted by vertical purple markers for Form A and by vertical green markers for Form L. (For interpretation of the references to colour in this figure legend, the reader is referred to the Web version of this article.)

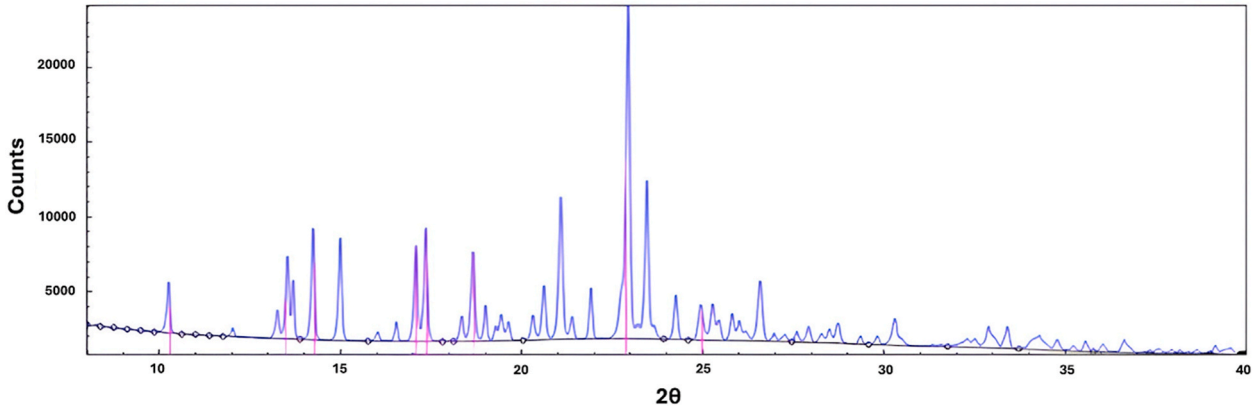

Fig. 8. Powder X-ray diffraction pattern of Batch 2, with the positions of specific and characteristic peaks, as reported in the patent for Form L [12], highlighted by vertical purple markers. (For interpretation of the references to colour in this figure legend, the reader is referred to the Web version of this article.)

Table 1
Unit cell and crystallographic parameters for Batch 2.

Crystal data	
Chemical formula	$C_{24}H_{23}FN_4O_3$
Crystal system	Monoclinic
Space group	$P2_1/c$
Cell parameters (Å,°)	a = 11.8601 (14)
	b = 8.0933 (10)
	c = 21.637 (3)
	β = 99.080 (2)
Volume (Å^3)	2050.9 (9)
Z	4

which is often correlated with faster dissolution rates. Faster dissolution in gastrointestinal fluids can lead to improved bioavailability, assuming other formulation factors (like solubility) are favorable. This is particularly important for a BCS class IV drug like OLA characterized by low aqueous solubility and low permeability, where surface area plays a critical role in achieving desired plasma concentrations. On the other hand, a formulator must keep in mind that powders with a higher surface area might also be more sensitive to moisture and other environmental factors, potentially affecting stability over time, and therefore careful handling and storage conditions might be required.

3.1.4. SEM analysis of powders from batch 1 and batch 2

The morphology of the two powder samples of OLA was investigated by SEM microscopy analysis. The key role of morphological studies is determined by the fact that they can provide essential information for pharmaceutical processing, especially for the development of solid dosage forms [28]. Indeed, numerous factors depend on the crystalline habit, such as particle orientation, powder fluidity, degree of packing, and even the dissolution profile of the powdered drug [35].

Fig. 10 shows that Batch 2 was composed of a single crystal family, with an irregular, parallelepiped-like shape that is repeated unchanged for all the crystallites analyzed. The size of the crystallites was also constant and comparable to each other (~5 μm) (Fig. 10A–B). On the other hand, Batch 1 presented a more heterogeneous composition in terms of crystallite shape and size. Although some of them were smaller in size (~2 μm) than those of the other sample, it has very large (~60 μm) and irregularly shaped aggregates (Fig. 10C–D). These differences in the morphology of the two samples of OLA can considerably affect the characteristics of the powders, such as the specific surface area and the dissolution rates, the different densities and compressibility. In fact, the presence of such large aggregates within the Batch 1 results in a smaller specific surface area (Table 2), going to slow down the rate of interaction with the solvent and decreasing the dissolution rate of the sample as discussed in the following. This aspect is important when a drug is a BCS class IV characterized by low solubility and low permeability. Furthermore, the presence of large aggregates lowers the level of compressibility of the powder and increases its total density, making it less workable and effective in the formulation phase.

Table 2
Density and specific surface area parameters of commercial powders in Batch 1 and 2.

SAMPLE	DENSITY (g/cm^3)	SPECIFIC SURFACE AREA (cm^3/g)
Batch 1	1.3819 ± 0.037	3823 ± 41
Batch 2	1.4163 ± 0.045	4320 ± 72

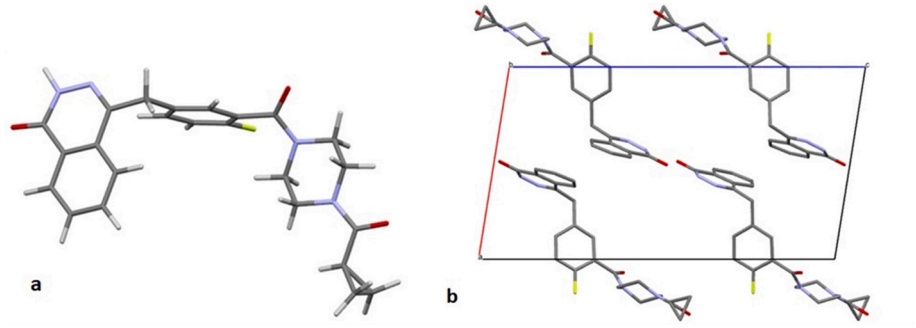

Fig. 9. The asymmetric unit of the Batch 2 compound (a); view of the packing of Batch 2 molecules along the b-axis. All hydrogen atoms have been removed for clarity (b). Color legend: carbon (light grey), hydrogen (white), oxygen (red), nitrogen (blue), sulfur (yellow), fluorine (green). (For interpretation of the references to colour in this figure legend, the reader is referred to the Web version of this article.)

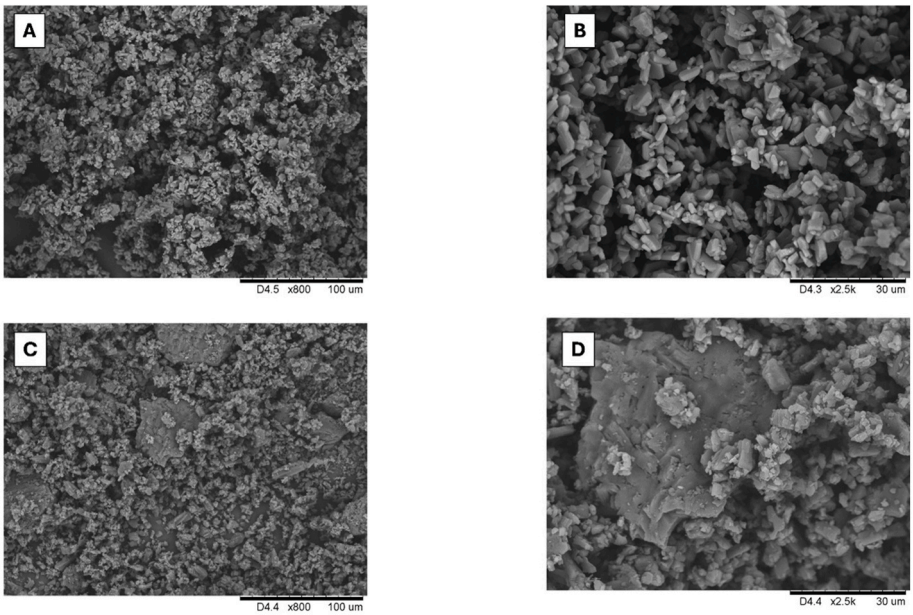

Fig. 10. SEM images of Batch 2 (A–B) and 1 (C–D) at different magnifications.

3.2. OLA behavior in aqueous environment

Based on the results obtained, which showed the presence of a mixture of Form A and Form L in Batch 1 and the pure polymorphic Form L in Batch 2, evaluated and clarified how different solid states of the samples could affect their micromeritic properties, we decided to also assess their behavior in an aqueous environment.

Preformulation studies of powders in an aqueous environment characterized by varying particle size and polymorphic compositions are of paramount importance in pharmaceutical development. The knowledge of fundamental properties of a drug in water, such as aqueous solubility and dissolution, is crucial for predicting drug bioavailability, optimizing formulation design, and ensuring consistent product performance. Differences in particle size and crystal structure can significantly impact on dissolution behavior of a drug, thereby affecting its rate and extent of absorption.

3.2.1. Equilibrium aqueous solubility of OLA

The equilibrium solubility of the powders from each sample was studied in water for 7 days at two different temperatures, 25 and 37 °C. As shown by the results reported in Fig. 11, after 24 h the equilibrium solubility was reached. The powder from Batch 1 exhibited a water solubility of 0.1239 ± 0.012 mg/mL (37 °C) and 0.0918 ± 0.008 mg/mL (25 °C), about twice that of the powder from Batch 2 (0.0609 ± 0.004 mg/mL at 37 °C and 0.0505 ± 0.003 mg/mL at 25 °C). These values remained approximately constant throughout the analysis period at each evaluated temperature. The results obtained are in agreement with the PXRD data, as the lower crystallinity of Batch 1 compared to Batch 2, results in higher drug solubility.

Consequently, the raw materials used could be crucial for the development of formulation, especially for oral dosage forms. The higher solubility of OLA in Batch 1 suggests that formulations utilizing this powder may result in better bioavailability, potentially enhancing drug absorption in the gastrointestinal tract. This is particularly beneficial for OLA, given its low bioavailability.

3.2.2. Dissolution profile of the powders in water

The influence of the different granulometry of Batch 1 and Batch 2 on the drug release profile was assessed through various dissolution studies conducted on the powders. Dissolution studies of the two powders were performed both at 37 °C in an aqueous environment for 8 h and in an acidic environment simulating the pH conditions of the gastric tract for 2 h. The results show that the powder from Batch 2 dissolved faster than that from Batch 1 (Fig. 12A). Specifically, in an aqueous environment, 90 % of drug dissolution was achieved by the powder from Batch 2, while 75 % of drug dissolution was showed for the other sample after 8

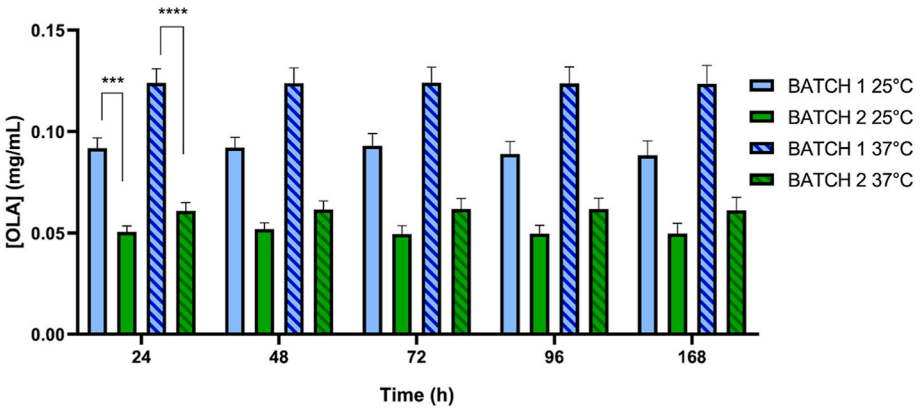

Fig. 11. Equilibrium aqueous solubility of powders of Batch 1 and 2 at 25 and 37 °C measured from 24 to 168 h (7 days). Results are shown as mean ± SD (n = 3).

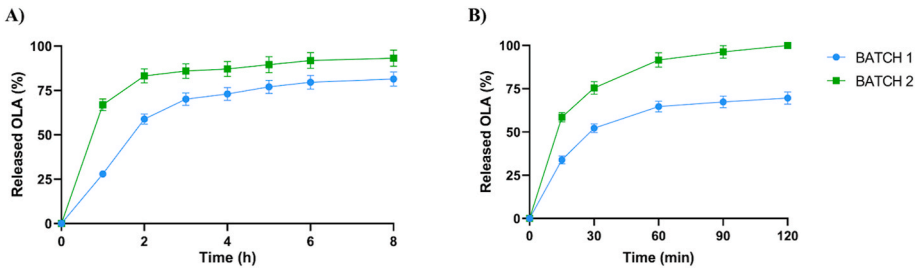

Fig. 12. Study of the dissolution rates of powders from Batch 1 and 2: (A) in water for 8h and (B) in 0.1 M HCl (pH 1.2) for 2h. Results are shown as mean ± SD (n = 3).

h. This trend was also confirmed in an acidic environment, where powder in Batch 1 achieved around 70 % of drug dissolution at 2 h, against the 100 % observed for Batch 2. This behavior contrasts with the solubility results and the higher crystallinity of Batch 2. These findings can be explained by the differences in particle size distribution between the two powders, as observed in the SEM analysis. The sample containing pure Form L showed a more uniform and finer particle size distribution, resulting in a larger surface area exposed to the aqueous solvent (Fig. 10). Consequently, the dissolution rate of Batch 2 was significantly higher compared to Batch 1.

3.2.3. *Intrinsic dissolution rate profile of the powders in water*

The evaluation of the IDR of the drug was carried out following compaction of the powders in Batch 1 and 2 to form a compressed surface area exposed to the solvent water. This allowed us to exclude the physical characteristics of the powder (such as granulometry and specific surface area) from the dissolution evaluation, ensuring that differences in dissolution rates are attributable only to the intrinsic properties of the drug (i.e. the presence of polymorphs). In fact, compaction renders porosity and powder density irrelevant, factors that may influence drug release rates depending on the resistance of the powder to solvent penetration [36]. The results in Fig. 13 showed that powder in Batch 1 exhibited almost double IDR in the aqueous medium (26.74 $mg/cm^2 \cdot min^{-1}$) compared to powder in Batch 2 (13.13 $mg/cm^2 \cdot min^{-1}$). This behaviour exhibited by sample could be due to the lower crystallinity of powder in Batch 1, which makes also the drug more soluble, confirming the results already observed in the aqueous solubility evaluation described previously. Indeed, it is well known that the dissolution process is explained by the second law of thermodynamics, whereby dissolution can be interpreted in thermodynamic terms as a transition driven by entropy increase, where the breaking of solute–solute interactions and the formation of solute–solvent interactions promote solubilization [37]. In our case, the higher solubility and IDR observed for the powder in Batch 1 (a mixture of Form L and the less crystalline Form A) is consistent with the likely metastable nature of

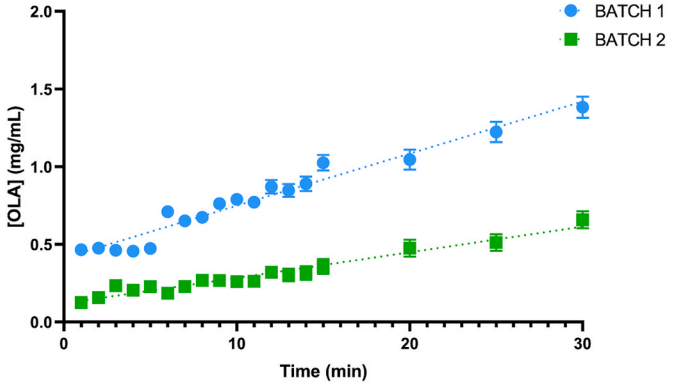

Fig. 13. Intrinsic dissolution profiles of powders from Batch 1 and Batch 2 at 37 °C. Results are shown as mean ± SD (n = 3).

polymorph A, while the more crystalline and less soluble Form L (in Batch 2) is likely the thermodynamically stable form under ambient conditions, despite transforming into Form An upon heating. This behaviour reflects greater thermal stability of Form A in the solid state, but not necessarily lower free energy in aqueous solution. IDR is a critical parameter in the development of solid dosage forms. The results showed in this study highlight that the properties of a powder (particle size, surface area, polymorphism) can differ from one batch to another and impact on its dissolution. The determination of IDR of both the batches can help a formulator during the early development phase of a dosage form. IDR is directly related to the bioavailability of a drug, as a higher dissolution rate indicates that the drug could dissolve more rapidly in the gastrointestinal tract after oral administration of a dosage form [38]. From an industrial point of view, the IDR is important to measure compounds that suffer from limited solubility and absorption to better understand formulation aspects that may allow its complete dissolution during the transit time of the gastrointestinal tract. The results observed in this study show that for both the powders the IDR values do not present criticality, since they are greater than 1 $mg/cm^2 \cdot min^{-1}$, a value considered limiting for bioavailability purposes. On the contrary, the criticality is observed on solubility, as in both batches a very low value was found such as to classify OLA as a BCS class IV. For this reason, a solubility study in the presence of solubilizing agents has been undertaken.

3.3. *Phase solubility in the presence of HP-β-CD and SOL*

The potential to enhance the aqueous solubility of OLA by solubilizing agents was evaluated for both batches in water at 37 °C over a 72-h period. The equilibrium solubility values obtained in the presence of increasing concentrations of HP-β-CD and SOL are presented in Fig. 14a–d. As shown in the graphs, OLA solubility was strongly influenced by both the type and concentration of solubilizing agent. In the case of HP-β-CD, a moderate but progressive increase in solubility was observed for both samples over time, reaching a plateau. This enhancement is attributed to the well-known ability of CDs to form inclusion complexes with hydrophobic drug molecules in aqueous media [39,40].

Specifically, at the highest HP-β-CD concentration used, OLA solubility increased by 12-fold for Batch 1 and 26-fold for Batch 2 compared to their initial equilibrium solubility (S_0) (Fig. 14a-b). Interestingly, despite the differences in crystalline form and solid-state characteristics between the two batches, both ultimately reached approximately the same final concentration of 1.5 mg/mL. This suggests that HP-β-CD effectively can eliminate solubility differences due to the initial solid state of the drug, likely through the formation of stable host–guest complexes that shield the hydrophobic regions of OLA and promote its dissolution.

The solubilizing effect of SOL was also investigated. SOL is an amphiphilic polymer known for its micelle-forming properties, hydrogen bonding capacity, and precipitation inhibition effects. Above its critical micellar concentration (CMC, 7.6 mg/L) [41], SOL can form

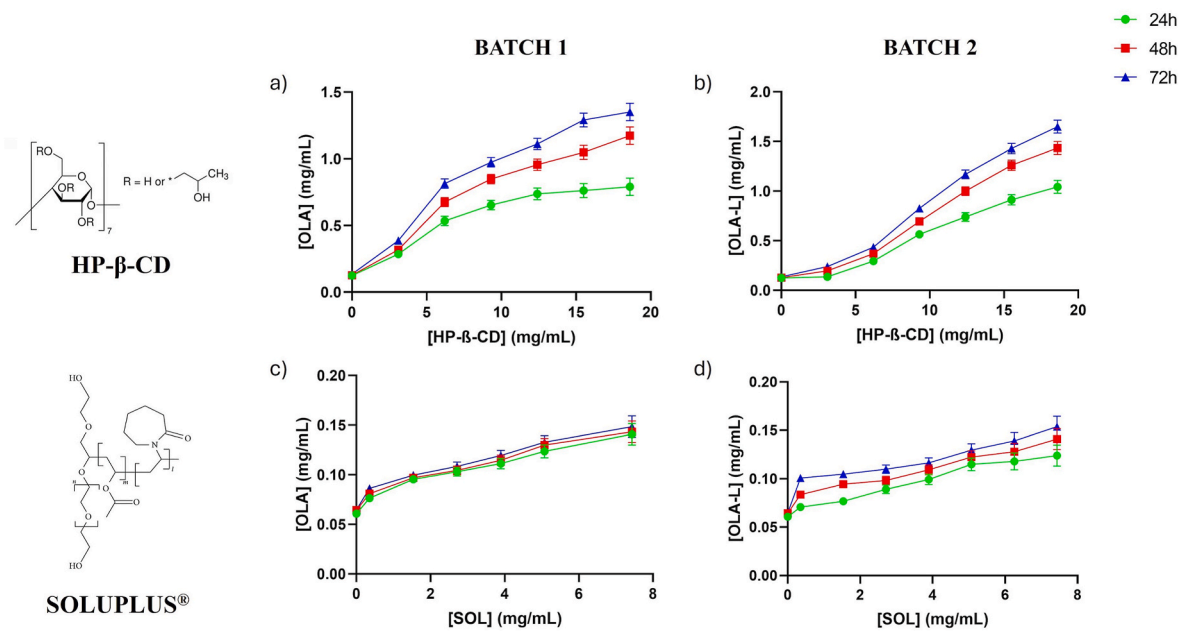

Fig. 14. Phase solubility diagrams of the powders from Batch 1 (a,c) and 2 (b,d) in the presence of increasing concentrations of HP-β-CD and SOL at 37 °C at 24, 48, and 72 h. All analyses were performed in triplicate.

micelles, facilitating drug solubilization [42,43]. Additionally, SOL can inhibit nucleation and crystal growth, thereby stabilizing the drug in a supersaturated state via steric hindrance [44]. Its viscoelastic properties also make it suitable for hot melt extrusion, expanding its utility in both liquid and solid dosage forms [45]. As shown in Fig. 14c–d, in the presence of SOL, OLA solubility increased by 1.2-fold for Batch 1 and 2.5-fold for Batch 2 after 72 h. Although this enhancement was less pronounced than that observed with HP-β-CD, SOL effectively brought both batches to the same final drug concentration of approximately 0.150 mg/mL, again minimizing differences attributable to their solid-state form.

These findings demonstrate that both HP-β-CD and SOL improve the solubility of OLA, albeit via different mechanisms: inclusion complexation in the case of HP-β-CD, and micellar solubilization plus stabilization effects in the case of SOL. The fact that both excipients eliminated initial solubility differences between the batches further supports their potential role in standardizing drug performance, regardless of polymorphic form. Since OLA belongs to BCS Class IV, characterized by low solubility and low permeability, improving aqueous solubility is a key strategy for increasing bioavailability. Enhanced solubility can reduce required doses, minimize side effects, and shorten exposure to P-glycoprotein efflux in the gastrointestinal tract, improving absorption [46]. Therefore, the use of such solubilizing agents could overcome the bioavailability problems exhibited by the polymorph Form L, which notoriously restricts the use of drug batches at industrial production level [15]. Finally, the distinct and complementary mechanisms of HP-β-CD and SOL suggest that their combined use could be a promising approach for formulation development. Future *in vitro* and *in vivo* studies are warranted to further explore this strategy.

4. Conclusions

This study underscores the relevance of thorough solid-state characterisation in evaluating APIs obtained from commercial suppliers. Despite identical chemical purity, the two OLA batches analyzed exhibited distinct polymorphic compositions - Batch 1 containing a mixture of Forms A and L, and Batch 2 consisting exclusively of Form L. These differences were associated with variations in equilibrium solubility and IDR, highlighting the impact of polymorphism on the biopharmaceutical performance of the drug. Micromeritics differences in particle size, specific surface area, and powder density were also identified, explaining the different powder dissolution observed in water.

Although no solid excipients or manufacturing processes were investigated, the use of HP-β-CD and SOL as solubilizing agents in aqueous media significantly enhanced OLA solubility, effectively minimizing batch-to-batch variability. These findings support the need for early assessment of solid-state properties and rational excipient selection during formulation development, particularly for poorly soluble drugs. Such approaches can help ensure consistent product performance and inform strategic formulation design.

CRediT authorship contribution statement

Giuseppe Francesco Racaniello: Writing – original draft, Methodology, Investigation, Conceptualization. **Monica Pistone:** Writing – original draft, Methodology, Investigation. **Annalisa Cutrignelli:** Writing – review & editing, Methodology, Data curation. **Corrado Cuocci:** Investigation, Data curation. **Rosanna Rizzi:** Writing – original draft, Formal analysis, Data curation. **Nunzio Denora:** Writing – review & editing, Supervision, Funding acquisition. **Antonio Lopalco:** Writing – review & editing, Supervision, Conceptualization. **Angela Assunta Lopedota:** Writing – review & editing, Supervision, Conceptualization.

Data availability

The datasets generated during and/or analyzed during the current study are available from the corresponding author on reasonable request.

Funding

This research received no external founding from agencies in the public, commercial or not-for-profit sectors.

Declaration of competing interest

The authors declare that they have no known competing financial

interests or personal relationships that could have appeared to influence the work reported in this paper.

Acknowledgments

The authors gratefully acknowledge the University of Bari (Italy). This work was partially funded by the Ministry of Economic Development funded project "GENESI" code 092-Prog n. F/180003/03/X43 for the development of innovative radiopharmaceuticals and biomarkers for the diagnosis of cancers of the male and female reproductive system (2021–2023); and (b) P.O.N "Ricerca e Innovazione" 2014–2020 - Fondi D.M. 1062/2021. Authors thank Mr. Pasquale Trotti for his advice and contribution for SEM analyses. The authors thank Mr. Francesco Baldassarre from Crystallography Institute, IC-CNR of Bari for his advice and contribution.

Appendix A. Supplementary data

Supplementary data to this article can be found online at https://doi.org/10.1016/j.jddst.2025.107123.

References

[1] E. Lau, Preformulation studies, in: Sep Sci Technol, Elsevier, 2001, pp. 173–233.
[2] S.S. Bharate, R.A. Vishwakarma, Impact of preformulation on drug development, Expet Opin. Drug Deliv. 10 (2013) 1239–1257, https://doi.org/10.1517/17425247.2013.783563.
[3] G. Verma, M.K. Mishra, Pharmaceutical preformulation studies in formulation and development of new dosage form: a review, Int. J. Pharm. Rev. Res. 5 (2016).
[4] J.W. Johannes, L. Almeida, K. Daly, A.D. Ferguson, S.E. Grosskurth, H. Guan, T. Howard, S. Ioannidis, S. Kazmirski, M.L. Lamb, N.A. Larsen, P.D. Lyne, K. Mikule, C. Ogoe, B. Peng, P. Petteruti, J.A. Read, N. Su, M. Sylvester, S. Throner, W. Wang, X. Wang, J. Wu, Q. Ye, Y. Yu, X. Zheng, D.A. Scott, Discovery of AZ0108, an orally bioavailable phthalazinone PARP inhibitor that blocks centrosome clustering, Bioorg. Med. Chem. Lett 25 (2015) 5743–5747, https://doi.org/10.1016/j.bmcl.2015.10.079.
[5] T. Yun, S. Lee, S. Yun, D. Cho, K. Bang, K. Kim, Investigation of stabilized amorphous solid dispersions to improve oral olaparib absorption, Pharmaceutics 16 (2024) 958, https://doi.org/10.3390/pharmaceutics16070958.
[6] A.D. Pathade, N. Kommineni, U. Bulbake, M.M. Thummar, G. Samanthula, W. Khan, Preparation and comparison of oral bioavailability for different nano-formulations of olaparib, AAPS PharmSciTech 20 (2019), https://doi.org/10.1208/s12249-019-1468-y.
[7] B. Rey, A. W, F.E. Souza, A. Bhattacharyya, Khalili, Crystalline Form of Olaparib, 2020.
[8] M. Friedlander, S. Banerjee, L. Mileshkin, C. Scott, C. Shannon, J. Goh, Practical guidance on the use of olaparib capsules as maintenance therapy for women with BRCA mutations and platinum-sensitive recurrent ovarian cancer, Asia Pac. J. Clin. Oncol. 12 (2016) 323–331, https://doi.org/10.1111/ajco.12636.
[9] E. Pujade-Lauraine, J.A. Ledermann, F. Selle, V. Gebski, R.T. Penson, A.M. Oza, J. Korach, T. Huzarski, A. Poveda, S. Pignata, M. Friedlander, N. Colombo, P. Harter, K. Fujiwara, I.L. Ray-Coquard, S. Banerjee, J. Liu, E.S. Lowe, R. Bloomfield, P. Pautier, J. Korach, T. Huzarski, T. Byrski, P. Pautier, P. Harter, N. Colombo, G. Scambia, M. Nicoletto, F. Nussey, A. Clamp, R. Penson, A. Poveda Velasco, M. Rodrigues, J.P. Lotz, F. Selle, D. Provencher, A. Prat Aparicio, L. Vidal Boixader, C. Scott, K. Tamura, M. Yunokawa, A. Lisyanskaya, J. Medioni, N. Pécuchet, C. Dubot, T. de la Motte Rouge, M.C. Kaminsky, B. Weber, A. Lortholary, C. Parkinson, J. Ledermann, S. Williams, S. Banerjee, J. Cosin, J. Hoffman, R. Penson, M. Plante, A. Covens, G. Sonke, F. Joly, A. Floquet, S. Banerjee, H. Hirte, A. Amit, T.W. Park-Simon, K. Matsumoto, S. Tjulandin, J. H. Kim, L. Gladieff, R. Sabbatini, D. O'Malley, P. Timmins, D. Kredentser, N. Laínez Milagro, M.P. Barretina Ginesta, A. Tibau Martorell, A. Gómez de Liaño Lista, B. Ojeda González, L. Mileshkin, M. Mandai, I. Boere, P. Ottevanger, J.H. Nam, E. Filho, S. Hamizi, F. Cognetti, D. Warshal, E. Dickson-Michelson, S. Kamelle, N. McKenzie, G. Rodriguez, D. Armstrong, E. Chalas, P. Celano, K. Behbakht, S. Davidson, S. Welch, L. Helpman, A. Fishman, I. Bruchim, M. Sikorska, A. Słowińska, W. Rogowski, M. Bidziński, B. Śpiewankiewicz, A. Casado Herraez, C. Mendiola Fernández, M. Gropp-Meier, T. Saito, K. Takehara, T. Enomoto, H. Watari, C.H. Choi, B.G. Kim, J.W. Kim, R. Hegg, I. Vergote, Olaparib tablets as maintenance therapy in patients with platinum-sensitive, relapsed ovarian cancer and a BRCA1/2 mutation (SOLO2/ENGOT-Ov21): a double-blind, randomised, placebo-controlled, phase 3 trial, Lancet Oncol. 18 (2017) 1274–1284, https://doi.org/10.1016/S1470-2045(17)30469-2.
[10] M. Robert, A. Patsouris, J.S. Frenel, C. Gourmelon, P. Augereau, M. Campone, Emerging PARP inhibitors for treating breast cancer, Expet Opin. Emerg. Drugs 23 (2018) 211–221, https://doi.org/10.1080/14728214.2018.1527900.
[11] Quigley Kathryn Anne, Still Ezra John, Chyall Leonard Jesse, 4-[3-(4-cyclopropanecarbonyl-piperazine-i-carbony-fluoro-benzyl*-2H-phthalazin-1-one, World Intellectual Property Organization, 2009.
[12] Keith Allan Menear, Phthalazinone Derivatives, vol. 8, US, 2012, 247,416 B2, A.P. O.D.J.L.M.R.H.
[13] European Medicines Agency (EMA), EPAR summary for Lynparza. https://www.ema.europa.eu/en/medicines/human/EPAR/lynparza, 2024. (Accessed 9 April 2025).
[14] D.L. Hughes, Patent review of manufacturing routes to recently approved PARP inhibitors: olaparib, Rucaparib, and Niraparib, Org. Process Res. Dev. 21 (2017) 1227–1244, https://doi.org/10.1021/acs.oprd.7b00235.
[15] Medicines and Healthcare products Regulatory Agency, Class 3 Medicines Recall: Lynparza Capsule 50mg (Olaparib), GOV.UK, 2018.
[16] V.N.P. Le, E. Robins, M.P. Flament, Air permeability of powder: a potential tool for dry powder inhaler formulation development, Eur. J. Pharm. Biopharm. 76 (2010) 464–469, https://doi.org/10.1016/j.ejpb.2010.09.003.
[17] A. Altomare, N. Corriero, C. Cuocci, A. Falcicchio, R. Rizzi, Solving a structure in the reciprocal space, real space and both by using the EXPO software, Crystals (Basel) 10 (2019) 16, https://doi.org/10.3390/cryst10010016.
[18] H.M. Rietveld, The Rietveld method, Phys. Scr. 89 (2014) 098002, https://doi.org/10.1088/0031-8949/89/9/098002.
[19] A. Altomare, G. Campi, C. Cuocci, L. Eriksson, C. Giacovazzo, A. Moliterni, R. Rizzi, P.-E. Werner, Advances in powder diffraction pattern indexing: *N-TREOR09*, J. Appl. Crystallogr. 42 (2009) 768–775, https://doi.org/10.1107/S0021889809025503.
[20] S.G. Zhukov, V.V. Chernyshev, E.V. Babaev, E.J. Sonneveld, H. Schenk, Application of simulated annealing approach for structure solution of molecular crystals from X-ray laboratory powder data, Z. Kristallogr. Cryst. Mater. 216 (2001) 5–9, https://doi.org/10.1524/zkri.216.1.5.18998.
[21] P. Giannozzi, S. Baroni, N. Bonini, M. Calandra, R. Car, C. Cavazzoni, D. Ceresoli, G.L. Chiarotti, M. Cococcioni, I. Dabo, A. Dal Corso, S. de Gironcoli, S. Fabris, G. Fratesi, R. Gebauer, U. Gerstmann, C. Gougoussis, A. Kokalj, M. Lazzeri, L. Martin-Samos, N. Marzari, F. Mauri, R. Mazzarello, S. Paolini, A. Pasquarello, L. Paulatto, C. Sbraccia, S. Scandolo, G. Sclauzero, A.P. Seitsonen, A. Smogunov, P. Umari, R.M. Wentzcovitch, Quantum ESPRESSO: a modular and open-source software project for quantum simulations of materials, J. Phys. Condens. Matter 21 (2009) 395502, https://doi.org/10.1088/0953-8984/21/39/395502.
[22] G. Prandini, A. Marrazzo, I.E. Castelli, N. Mounet, N. Marzari, Precision and efficiency in solid-state pseudopotential calculations, npj Comput. Mater. 4 (2018) 72, https://doi.org/10.1038/s41524-018-0127-2.
[23] S. Grimme, J. Antony, S. Ehrlich, H. Krieg, A consistent and accurate *ab initio* parametrization of density functional dispersion correction (DFT-D) for the 94 elements H-Pu, J. Chem. Phys. 132 (2010), https://doi.org/10.1063/1.3382344.
[24] J. van de Streek, M.A. Neumann, Validation of molecular crystal structures from powder diffraction data with dispersion-corrected density functional theory (DFT-D), Acta. Crystallogr. B Struct. Sci. Cryst. Eng. Mater 70 (2014) 1020–1032, https://doi.org/10.1107/S2052520614022902.
[25] L. Peltonen, P. Liljeroth, T. Heikkilä, K. Kontturi, J. Hirvonen, Dissolution testing of acetylsalicylic acid by a channel flow method—correlation to USP basket and intrinsic dissolution methods, Eur. J. Pharmaceut. Sci. 19 (2003) 395–401, https://doi.org/10.1016/S0928-0987(03)00140-4.
[26] A. Lopedota, A. Cutrignelli, A. Trapani, G. Boghetich, N. Denora, V. Laquintana, G. Trapani, G. Liso, Effects of different cyclodextrins on the morphology, loading and release properties of poly (DL-lactide-co-glycolide)-microparticles containing the hypnotic agent etizolam, J. Microencapsul. 24 (2007) 214–224, https://doi.org/10.1080/02652040601058152.
[27] A. Cutrignelli, F. Sanarica, A. Lopalco, A. Lopedota, V. Laquintana, M. Franco, B. Boccanegra, P. Mantuano, A. De Luca, N. Denora, Dasatinib/HP-β-CD inclusion complex based aqueous formulation as a promising tool for the treatment of paediatric neuromuscular disorders, Int. J. Mol. Sci. 20 (2019) 1–16, https://doi.org/10.3390/ijms20030591.
[28] G. Chawla, P. Gupta, R. Thilagavathi, A.K. Chakraborti, A.K. Bansal, Characterization of solid-state forms of celecoxib, Eur. J. Pharmaceut. Sci. 20 (2003) 305–317, https://doi.org/10.1016/S0928-0987(03)00201-X.
[29] X.L. Dai, B.W. Pang, W.T. Lv, J.F. Zhen, L. Gao, C.W. Li, J. Xiong, T.B. Lu, J. M. Chen, Improving the physicochemical and pharmacokinetic properties of olaparib through cocrystallization strategy, Int. J. Pharm. 647 (2023), https://doi.org/10.1016/j.ijpharm.2023.123497.
[30] R. Chadha, P. Arora, A. Saini, D. Jain, An insight into thermodynamic relationship between polymorphic forms of efavirenz, J. Pharm. Pharmaceut. Sci. 15 (2012) 234–251, https://doi.org/10.18433/J3J30Z.
[31] A.B. Anane-Adjei, E. Jacobs, S.C. Nash, S. Askin, R. Soundararajan, M. Kyobula, J. Booth, A. Campbell, Amorphous solid dispersions: utilization and challenges in preclinical drug development within AstraZeneca, Int. J. Pharm. 614 (2022) 121387, https://doi.org/10.1016/j.ijpharm.2021.121387.
[32] J.A. Baird, B. Van Eerdenbrugh, L.S. Taylor, A classification system to assess the crystallization tendency of organic molecules from undercooled melts, J. Pharmaceut. Sci. 99 (2010) 3787–3806, https://doi.org/10.1002/jps.22197.
[33] G. Perlovich, A. Surov, Polymorphism of monotropic forms: relationships between thermochemical and structural characteristics, Acta. Crystallogr. B Struct. Sci. Cryst. Eng. Mater 76 (2020) 65–75, https://doi.org/10.1107/S2052520619015671.
[34] H.P. Klug, L.E. Alexander, X-Ray Diffraction Procedures for Polycrystalline and Amorphous Materials, second ed., John Wiley and Sons, New York, 1974.
[35] A.K. Tiwary, Modification of crystal habit and its role in dosage form performance, Drug Dev. Ind. Pharm. 27 (2001) 699–709, https://doi.org/10.1081/DDC-100107327.
[36] K. Löbmann, K. Flouda, D. Qiu, T. Tsolakou, W. Wang, T. Rades, The influence of pressure on the intrinsic dissolution rate of amorphous Indomethacin,

Pharmaceutics 6 (2014) 481–493, https://doi.org/10.3390/pharmaceutics6030481.
[37] Y. Ren, J. Shen, K.X. Yu, C.U. Phan, G.X. Chen, J.Y. Liu, X. Hu, J.Y. Feng, Impact of crystal habit on solubility of ticagrelor, Crystals (Basel) 9 (2019), https://doi.org/10.3390/cryst9110556.
[38] A. Teleki, O. Nylander, C.A.S. Bergström, Intrinsic dissolution rate profiling of poorly water-soluble compounds in biorelevant dissolution media, Pharmaceutics 12 (2020), https://doi.org/10.3390/pharmaceutics12060493.
[39] P. Saokham, C. Muankaew, P. Jansook, T. Loftsson, Solubility of cyclodextrins and Drug/Cyclodextrin complexes, Molecules (Basel) 23 (2018) 1161, https://doi.org/10.3390/molecules23051161.
[40] A. Lopedota, A. Cutrignelli, V. Laquintana, N. Denora, R.M. Iacobazzi, M. Perrone, E. Fanizza, M. Mastrodonato, D. Mentino, A. Lopalco, N. Depalo, M. Franco, Spray dried chitosan microparticles for intravesical delivery of Celecoxib: preparation and characterization, Pharm. Res. 33 (2016) 2195–2208, https://doi.org/10.1007/s11095-016-1956-7.
[41] R. Pignatello, R. Corsaro, A. Bonaccorso, E. Zingale, C. Carbone, T. Musumeci, Soluplus® polymeric nanomicelles improve solubility of BCS-class II drugs, Drug. Deliv. Transl. Res. 12 (2022) 1991–2006, https://doi.org/10.1007/s13346-022-01182-x.
[42] C. Sofroniou, M. Baglioni, M. Mamusa, C. Resta, J. Doutch, J. Smets, P. Baglioni, Self-Assembly of soluplus in aqueous solutions: characterization and prospectives on perfume encapsulation, ACS Appl. Mater. Interfaces 14 (2022) 14791–14804, https://doi.org/10.1021/acsami.2c01087.
[43] M. Darwich, V. Mohylyuk, K. Kolter, R. Bodmeier, A. Dashevskiy, Enhancement of itraconazole solubility and release by hot-melt extrusion with soluplus®, J. Drug Deliv. Sci. Technol. 81 (2023) https://doi.org/10.1016/j.jddst.2023.104280.
[44] M.S. Attia, A. Elshahat, A. Hamdy, A.M. Fathi, M. Emad-Eldin, F.E.S. Ghazy, H. Chopra, T.M. Ibrahim, Soluplus® as a solubilizing excipient for poorly water-soluble drugs: recent advances in formulation strategies and pharmaceutical product features, J. Drug Deliv. Sci. Technol. 84 (2023), https://doi.org/10.1016/j.jddst.2023.104519.
[45] S.S. Gupta, T. Parikh, A.K. Meena, N. Mahajan, I. Vitez, A.T.M. Serajuddin, Effect of carbamazepine on viscoelastic properties and hot melt extrudability of soluplus®, Int. J. Pharm. 478 (2015) 232–239, https://doi.org/10.1016/j.ijpharm.2014.11.025.
[46] E. Pfuma, P. Zhao, Q. Liu, H. Li, L. Zhao. Clinical Pharmacology and Biopharmaceutics Review(S), 2014.